Noiseless nonreciprocity in a parametric active device

Archana Kamal,[1] John Clarke,[2] M. H. Devoret[1*]

[1]Department of Physics and Applied Physics, Yale University,
15 Prospect Street, New Haven, CT 06520, USA
[2]Department of Physics, University of California, and Materials Sciences Division,
Lawrence Berkeley National Laboratory, Berkeley, CA 94720, USA

[*]Correspondence to: M. H. Devoret[1] email: michel.devoret@yale.edu.

Nonreciprocal devices such as circulators and isolators belong to an important class of microwave components employed in applications like the measurement of mesoscopic circuits at cryogenic temperatures [1, 2, 3, 4]. The measurement protocols usually involve an amplification chain which relies on circulators to separate input and output channels and to suppress backaction from different stages on the sample under test. In these devices the usual reciprocal symmetry of circuits is broken by the phenomenon of Faraday rotation based on magnetic materials and fields [5]. However, magnets are averse to on-chip integration, and magnetic fields are deleterious to delicate superconducting devices [6, 7, 8]. Here we present a new proposal combining two stages of parametric modulation emulating the action of a circulator. It is devoid of magnetic components and suitable for on-chip integration. As the design is free of any dissipative elements and based on reversible operation, the device operates noiselessly, giving it an important advantage over other nonreciprocal active devices for quantum information processing applications.

Reciprocity is one of the fundamental symmetries frequently encountered in electrical circuits. It is equivalent to the more familiar notion of the principle of reversibility in optics which states that any experiment is symmetric under an exchange of source and image [9]. Reciprocity can, however, be violated, for example, by the magneto-optic effect of Faraday rotation [5] which leads to rotation of the polarization vector of light resulting from different propagation velocities of left- and right-circularly polarized waves in the presence of an applied magnetic field $\mathbf{B}$ parallel to the direction of propagation (Fig. 1). The nonreciprocal phenomenon of Faraday rotation should be contrasted with the superficially similar, though reciprocal, effect of optical activity where the polarization vector of light is rotated on passage through a non-centrosymmetric (chiral) medium. This change in the sense of rotation of polarization for counterpropagating waves in a Faraday medium (as seen by the observer receiving the light) has led some physicists to refer to this effect as a form of time-reversal-symmetry-breaking, a use of words that we prefer to avoid here [10, 11].

The phenomenon of nonreciprocity has propelled numerous theoretical investigations [[12] and refs. therein]; furthermore it offers immediate practical applications. Recent progress in solid state superconducting qubits, that provide some of the most promising architectures for scalable quantum computers [13, 14], has generated a huge incentive to integrate the components required for qubit operations and readout on-chip for incorporation in future quantum mechanical processors. A large variety of qubit readout protocols involve microwave reflection based measurements and rely on nonreciprocal devices like circulators (or isolators) for separation of input and output channels [1, 2]. These devices also play a strategic role in measurements based on low-noise microwave parametric amplifiers which, with the exception of designs based on the current-biased dc SQUID (Superconducting Quantum Interference Device), are also operated in a reflection mode with both the input and output signals collected on the same spatial channel [15, 16]. However, circulators (and isolators) routinely use bulk

components made from ferrites to achieve nonreciprocal phase shifts (Fig. 1c) through Faraday rotation, making them unamenable to chip fabrication. Moreover, to bias the magnetic field in the ferrite, most of these devices use a permanent magnet which may channel flux into the superconducting device under test.

In this letter, we present the full analysis of a model for a four-port circulator based on parametric active devices with no magnetic components. In active devices the energy source – provided by the pump – acts as the external "bias" field and sets the reference phase for the system, in analogy with the role played by the magnetic field in a Faraday medium. We exploit this effect in a cascade of active devices with pump phases at each stage tuned appropriately to obtain nonreciprocal transmission.

The main building block of our design is a reversible IQ (in-phase/quadrature) modulator capable of performing noiseless frequency up- and down-conversion. A convenient analytical model capturing the fundamental properties of the device is shown in Fig. 2a. The device comprises two low frequency LC resonators (addressed by two semi -infinite transmission lines A and B) coupled to a high frequency resonator (addressed by the transmission line C) through time-varying couplings M_1, M_2 that emulate the role of the pump drive in active nonlinear devices and transfer energy from the tone at ω_c to the signal modes propagating on the transmission lines. It operates in a manner analogous to the IQ modulation schemes routinely used in radiofrequency (RF) communication systems and microwave pulse engineering (hence the name) and converts two orthogonal spatial modes travelling on two distinct spatial ports (A, B) at same frequency (here ω_0) into two orthogonal temporal modes travelling on the same spatial line (C) at different frequencies (ω_+, ω_-). In view of the reversible frequency conversion performed by this device (Fig. 2a), we will henceforth refer to it as the up/down-converter (UDC). In practice, such a device can be implemented on-chip using a ring modulator based on Josephson junctions, along the lines of the recently demonstrated experiment with Josephson

parametric converter [17, 18].

The complete design for the active circulator (Fig. 3a) consists of a UDC functioning as a frequency up-converter, a phase-shifter and a second UDC functioning as a frequency down-converter.

A concise representation of the dynamics at each of the three stages in the cascade is provided by the scattering matrix S which relates the outgoing wave amplitudes to the incoming wave amplitudes as seen from the ports of a network. We start by deriving the scattering matrix of the UDC stage. This is done by evaluating the impedance matrix Z of the UDC, as seen from its ports, and using the identity [5]

$$S = (Z + Z_0)^{-1} \times (Z - Z_0) \tag{1}$$

where

$$Z_0 = \mathrm{diag}(Z_A, Z_B, Z_C, Z_C), \tag{2}$$

with $Z_A = Z_B$ and Z_C denoting the characteristic impedances of the semi-infinite transmission lines serving as low and high frequency ports respectively. We obtain (see supplementary information, Fig. S1)

$$\begin{pmatrix} a_0^{'\mathrm{out}} \\ a_0^{''\mathrm{out}} \\ b_+^{\mathrm{out}} \\ b_-^{\dagger\mathrm{out}} \end{pmatrix} = \begin{pmatrix} r_0 & -q_0 & t_d e^{-i\phi} & s_d e^{i\phi} \\ q_0 & r_0 & i t_d e^{-i\phi} & -i s_d e^{i\phi} \\ t_u e^{i\phi} & -i t_u e^{i\phi} & r_+ & 0 \\ -s_u e^{-i\phi} & -i s_u e^{-i\phi} & 0 & r_- \end{pmatrix} \begin{pmatrix} a_0^{'\mathrm{in}} \\ a_0^{''\mathrm{in}} \\ b_+^{\mathrm{in}} \\ b_-^{\dagger\mathrm{in}} \end{pmatrix}. \tag{3}$$

Here a and b denote the (reduced) amplitudes or the annihilation operators for the waves travelling on left and right transmission lines respectively (see supplementary information for details). These satisfy bosonic commutation relations of the form [19]

$$[a_i, a_j^\dagger] = \delta(\omega_i - \omega_j). \tag{4}$$

In writing Eqs. (3) and (4), we have set $a_0 = a[\omega_0], a_+ = a[\omega_+], a_- = a[\omega_-]$ (see Fig. 2b). Similarly, the reflection coefficients at various ports are denoted by r_0, r_+ and r_-. The cross

reflection between the low frequency signal ports is denoted by q_0. The transmission coefficients are written as t (transmission without conjugation) and s (transmission with conjugation) with subscripts (u, d) indicating the up-conversion and down-conversion respectively. It is useful to note that the phase of the carrier, denoted by ϕ, affects only the transmitted amplitudes and rotates the two sidebands in opposite directions as can be seen from the corresponding scattering coefficients s and t in Eq. (3). The invariance of reflection amplitudes to the phase of the coupling will be important in understanding total reflections of the cascade, as we describe later.

Further, we note that the matrix obtained in Eq. (3) is non-unitary, that is $S^\dagger S \neq 1$, which implies nonconservation of photon number as is natural for an active device. The matrix recovers its unitary form as we turn off the couplings $M_1,\ M_2$ responsible for energy transfer between the pump and the signal modes. The full 8×8 matrix [supplementary information, Eq. (S18)], describing the device operation for all modes and their respective conjugates, fulfils the fundamental requirement of *symplecticity*[17].

We can similarly describe the action of the frequency-independent phase shifting (PS) stage using a scattering matrix of the form

$$\begin{pmatrix} a_+^{\rm out} \\ a_-^{\dagger \rm out} \\ b_+^{\rm out} \\ b_-^{\dagger \rm out} \end{pmatrix} = \begin{pmatrix} 0 & 0 & e^{-i\theta} & 0 \\ 0 & 0 & 0 & e^{i\theta} \\ e^{-i\theta} & 0 & 0 & 0 \\ 0 & e^{i\theta} & 0 & 0 \end{pmatrix} \begin{pmatrix} a_+^{\rm in} \\ a_-^{\dagger \rm in} \\ b_+^{\rm in} \\ b_-^{\dagger \rm in} \end{pmatrix}. \tag{5}$$

For each stage of the cascade, we now go from the scattering matrix representation to the transfer matrix representation [5],

$$\begin{pmatrix} a_+^{\rm out} \\ a_-^{\dagger \rm out} \\ b_+^{\rm out} \\ b_-^{\dagger \rm out} \end{pmatrix} = S \begin{pmatrix} a_+^{\rm in} \\ a_-^{\dagger \rm in} \\ b_+^{\rm in} \\ b_-^{\dagger \rm in} \end{pmatrix} \quad \mapsto \quad \begin{pmatrix} b_+^{\rm out} \\ b_+^{\rm in} \\ b_-^{\dagger \rm out} \\ b_-^{\dagger \rm in} \end{pmatrix} = T \begin{pmatrix} a_+^{\rm in} \\ a_+^{\rm out} \\ a_-^{\dagger \rm in} \\ a_-^{\dagger \rm out} \end{pmatrix}, \tag{6}$$

since it is straightforward to calculate the total transfer matrix of the device by multiplying the

respective transfer matrices of different stages [20],

$$T_{\text{total}} = T_{DC_R} \times T_{PS} \times T_{UC_L}. \tag{7}$$

Here the subscripts L, R index the left hand upconversion (UC) and right hand downconversion (DC) stage (Fig. 3a). The scattering matrix of the whole device is then obtained from T_{total} using the inverse of the transformation in Eq. (6) (see supplementary information). We also note that

$$\begin{aligned} T_{DC} &= F^{-1} \times T_{UC}^{-1} \times F \\ &= F \times T_{UC}^{-1} \times F, \ \ (F^{-1} = F) \end{aligned} \tag{8}$$

where $F = \sigma_X \otimes I_2$, (σ_X is the 2D pauli spin matrix and I_2 is the 2D unity matrix). This matrix F is required to flip the indices, thus maintaining consistency in labelling the 'in' and 'out' amplitudes along a given direction of propagation.

In our analysis we consider the operation at resonance, that is, when the input signal frequency coincides with the band center of the input resonators. Setting the phase of the pump at the first UDC stage $\phi_L = 0$ for calculational simplicity, we observe a transmission resonance for $\theta = \pm\pi/2$ (phase rotation by the PS stage), $\phi_R = \pi/4$ (phase of the pump at the second UDC stage), $\delta_\pm = 1/\sqrt{2}$ (detuning of the sidebands from the carrier in units of linewidth i.e. half width at full maximum of the resonance lineshape) of the high frequency resonator), and $\alpha_L = \alpha_R = M_0/\sqrt{L_{A,B}L_C} = 2^{-3/4}$ (strength of the parametric coupling). For this choice of parameters, we obtain the scattering matrix of the complete device as

$$S_{\text{total}} = \begin{pmatrix} 0 & 0 & 0 & i \\ 0 & 0 & -i & 0 \\ i & 0 & 0 & 0 \\ 0 & i & 0 & 0 \end{pmatrix}. \tag{9}$$

This is the matrix of a perfect four-port circulator. The analogy between a conventional circulator and the active circulator design proposed in this paper is made apparent from the respective

wave propagation diagrams in Figs. 1c and 3b (see supplementary information for details on the calculation of coefficients on different arms in 3b). Nonetheless there are important differences between the two designs despite the identity of the final S matrix. The coefficients on the forward (green) and backward (red) propagating arms of the active circulator design (Fig. 3b) involve deamplification followed by amplification, unlike the passive splitters (90 or 180 degree hybrids) employed in Faraday rotation schemes. This can be observed by squaring the amplitudes on each of the two arms originating from (or terminating into) a port and calculating the net power output, for each isolated UDC stage. It is straightforward to observe that, unlike the case of Fig. 1c, they do not add up to unity. Nonetheless, the overall transmission is unity due to an exact cancellation of the reduction and gain in amplitudes. The wave propagation diagrams in Fig. 3b reveal another important difference of this design from that of a conventional circulator. The non-reciprocal action of the active circulator is not based upon any non-reciprocal phase shifters; instead it relies on the active stages used for frequency up- and down-conversion. The phase matching condition in the forward direction is met by tuning the phase of the coupling at the input and output UDC stages. In the reverse direction the phase mismatch leads to unity transmission in the spatially orthogonal port instead, leading to complete isolation between the incident signal port and its corresponding output port.

Fig. 3c shows a convenient method to visualize this circulator action geometrically by mapping the device dynamics at different stages using a modulation ellipse. This approach is inspired by the polarization ellipse used to represent of state of polarization of an electromagnetic wave (linear, circular or elliptical), which involves recording the trajectory traced out by the tip of the polarization vector of light (defined by the instantaneous direction of the electric field vector **E**) in a plane perpendicular to the direction of propagation. Equivalently, a two-dimensional representation of the components E_X and E_Y of the electric field in the complex plane can be used to obtain a geometric description of the polarization of the light wave. In

the case of a modulation ellipse representation of the dynamics of the proposed device, we extend this idea to map *two* distinct orthogonal modes (x,y) at each stage of the device [spatial: $(x = a_0^{'}, y = a_0^{''})$ or temporal: $(x = a_+, y = a_-)$] as an ellipse in the plane defined by the coordinates $I = Re[x+y], Q = Im[x-y^*]$. This exercise shows that the final ellipses obtained at the output in case of forward and backward propagation through the device are rotated by 90 degrees with respect to each other. This indicates that in the case of reverse propagation the orthogonal spatial port, relative to the forward propagation, receives the transmitted energy leading to a circulator action (see supplementary information and Fig. S2 for more details).

Furthermore, as seen from Eq. (3), the reflection coefficients at the UDC stages are non-zero for all modes. However, for the whole cascade, the total reflection is identically zero at every port [$s_{ii} = 0$ for all i in Eq. (9)]. This remarkable cancellation of total reflections for the cascade can be understood in analogy with a Fabry-Perot resonance where a cavity flanked by two identical reflecting mirrors displays unity transmission at resonance. The total phase shift between the active "mirrors" in our device: $(\pi/2)_{a_+} - (-\pi/2)_{a_-^\dagger} = \pi$, is akin to the resonance condition when a half-wavelength of the incident radiation equals the length of the Fabry-Perot cavity. Also the reflections at the two UDC stages are identical [as the reflection coefficients are independent of the phase angle ϕ, cf. Eq. (3)], fulfilling the second condition for the transmission resonance and net cancellation of reflections [21].

We show the dependence of circulator action on different parameters in the device in Fig. 4. Since the isolation achieved is robust to reasonable deviations of parameters from their ideal values ($\phi_L = 0,\ \phi_R = \pi/4,\ \theta = \pi/2,\ \delta_\pm = 1/\sqrt{2},\ \alpha_L = \alpha_R = 2^{-3/4}$), the active circulator design holds promise for use in practical circuits. Another interesting feature of this device is the reversal of transmission characteristics with phase of the pumps ($\phi_{L,R} \mapsto -\phi_{L,R}$) (Fig. 4c). In the classic circulators based on passive Faraday rotation, this can be accomplished by changing the polarity of the magnetic bias field. Thus the clock ("pump phase") in an active

device indeed plays a role equivalent to the magnetic field in a Faraday medium.

In conclusion, we have described a scheme for achieving nonreciprocal wave propagation using a protocol involving up-conversion followed by down-conversion mediated by an appropriate phase shift [22]. The proposed design performs noiselessly as it consists of purely dispersive components with no dissipation, making it attractive for quantum information applications using superconducting circuits [23]. Besides microwave applications, the architecture of the protocol described in this paper can be adapted to optical frequencies, where it can complement the recently proposed designs of nonreciprocal light propagation based on dynamical modulation of the refractive index of photonic structures [24] and the use of a surface waveguide on photonic crystals [25]. In addition to the practical applications outlined above, the treatment described in this letter may also give theoretical insights into the inherently directional dynamics of devices like the dc SQUID [26], when additional active stages are included in the chain. This can be useful in tackling unanswered questions pertaining to the quantum noise of dc SQUID amplifiers [27].

References

[1] Wallraff, A. *et al.* Strong coupling of a single photon to a superconducting qubit using circuit quantum electrodynamics. *Nature*, 431:162, 2004.

[2] Mallet, F. *et al.* Single-shot qubit readout in circuit quantum electrodynamics. *Nat Phys*, 5:791–795, 2009.

[3] Johnson, B. R. *et. al.* Quantum non-demolition detection of single microwave photons in a circuit. *Nat. Phys.*, 6:1745–2473, 2010.

[4] Naaman, O., Aumentado, J., Friedland, L., Wurtele, J. S. & Siddiqi, I. Phase-locking transition in a chirped superconducting josephson resonator. *Phys. Rev. Lett.*, 101(11):117005, 2008.

[5] Pozar, David M. *Microwave Engineering*, pages 471–482. Wiley, ed. 3, 2005.

[6] Van Harlingen, D. J. *et. al.* Decoherence in Josephson-junction qubits due to critical-current fluctuations. *Phys. Rev. B*, 70(6):064517, 2004.

[7] Kakuyanagi, K. *et. al.* Dephasing of a superconducting flux qubit. *Phys. Rev. Lett.*, 98(4):047004, 2007.

[8] Choi, S., Lee, D.-H., Louie, S. G. & Clarke, J. Localization of metal-induced gap states at the metal-insulator interface: Origin of flux noise in squids and superconducting qubits. *Phys. Rev. Lett.*, 103(19):197001, 2009.

[9] Schuster, A. *An Introduction to the Theory of Optics*, pages 41–45. Edward Arnold, London, 1904.

[10] Barron, L. D. Parity and Optical Activity. *Nature*, 238:17–19, 1972.

[11] This confusion can be resolved by considering the symmetries of $\mathbf{E}$ and $\mathbf{B}$ fields under parity (P) and time reversal (T) operations. The electric field E described by a *polar vector* that is *symmetric under time reversal* and the magnetic field B described by an *axial vector* (more appropriately as an antisymmetric tensor of rank two) that is *anti-symmetric under time reversal* lead to the invariance of Maxwell's equations describing the electromagnetic field under both P and T operations. Thus any physical process involving only electromagnetic interactions also preserves these two symmetries. In other words, if P and T are applied to a *complete* experiment, the resulting situation should also be

physically realizable as a solution of Maxwell's equations. It can be checked that Faraday rotation under both P and T operations leads to feasible outcomes, thus preserving both the symmetries.

[12] Potton, R. J. Reciprocity in optics. *Rep. Prog. Phys.*, 67:717–754, 2004.

[13] Ladd, T. D. *et al.* Quantum computers. *Nature*, 464:45–53, 2010.

[14] Clarke, J. & Wilhelm, F. K. Superconducting quantum bits. *Nature*, 453:1031–1042, 2008.

[15] Castellanos-Beltran, M. A. & Lehnert, K. W. Widely tunable parametric amplifier based on a superconducting quantum interference device array resonator. *Appl. Phys. Lett.*, 91(8):083509, 2007.

[16] Yamamoto, T. *et al.* Flux-driven josephson parametric amplifier. *Appl. Phys. Lett.*, 93(4):042510, 2008.

[17] Bergeal, N *et al.* Analog information processing at the quantum limit with a josephson ring modulator. *Nat Phys*, 6:296–302, 2010.

[18] Bergeal, N. *et al.* Phase preserving amplification near the quantum limit with a Josephson Ring Modulator. available at http://arxiv.org/abs/arXiv:0912.3407.

[19] Yurke, B. Input output theory. In Drummond, P.D. & Ficek, Z., editor, *Quantum Squeezing*, pages 53–95. Springer, 2004.

[20] We note that for the case of IQ coupling considered in Fig. 2(A), the terms coupling the two sidebands, s_{34} and s_{43}, are zero [Eq. (3)]. If the phase difference between the two couplings M_1 and M_2 deviates from 90 degrees, crosstalk appears between the two

sidebands generated at port C. Furthermore, if M_1 and M_2 would be completely in phase, the two sidebands would be maximally coupled while the cross reflections q_0 between the low frequency input ports would reduce to zero. In such a case, the transformation defining the transfer matrix is singular (refer to methods under supplementary information for details).

[21] A point of disticntion between the two pictures is that the symmetry of the active circulator design is described by a sub-group of the $SU(4)$ group (the group formed by 4×4 complex matrices of unit determinant, Eq. 9]), and not by the $SU(2)$ group that describes passive lossless two-port devices like the Fabry-Perot resonator.

[22] A recent theoretical work [28] showed the existence of a non-reciprocal effect using non-linear circuit that involves microwave resonators coupled through Josephson junctions. While the proposal of this reference is based on a passive Josephson circuit, it involves, unlike our proposal, very small JJ susceptible to offset charges. Furthermore, due to its small characteristic energy, that device will handle the qubit readout signals with a lesser throughput than our proposed device.

[23] DiCarlo, L. *et. al.* Demonstration of two-qubit algorithms with a superconducting quantum processor. *Nature*, 460:240–244, 2009.

[24] Yu, Z. & Fan, S. Complete optical isolation created by indirect interband photonic transitions. *Nature Photonics*, 3:91–94, 2009.

[25] Liu, A. Q., Khoo, E. H., Cheng, T. H., Li, E. P. & Li, J. A frequency-selective circulator via mode coupling between surface waveguide and resonators. *Appl. Phys. Lett.*, 92(2):021119, 2008.

[26] Clarke, J. & Braginsky, A. I., editor. *The SQUID Handbook Vol. I Fundamentals and Technology of SQUIDs and SQUID Systems*. Wiley-VCH Verlag GmbH and Co. KGaA, 2004.

[27] Clarke, J. & Braginsky, A. I., editor. *The SQUID Handbook Vol. II Applications of SQUIDs and SQUID Systems*. Wiley-VCH Verlag GmbH and Co. KGaA, 2006.

[28] Koch, J., Houck, A. A., Le Hur, K. & Girvin, S. M. Time-reversal symmetry breaking in circuit-QED based photon lattices. *arXiv:1006.0762*, 2010.

Acknowledgements

We acknowledge useful discussions with S. M. Girvin, Jens Koch and R. J. Schoelkopf. This research was supported by the US National Security Agency through the US Army Research Office grant W911NF-05-01-0365, the W. M. Keck Foundation, the US National Science Foundation through grant DMR-032-5580 (A.K. and M.H.D.) as well as by the Director, Office of Science, Office of Basic Energy Sciences, Materials Sciences and Engineering Division, of the U.S. Department of Energy under Contract No. DE-AC02- 05CH11231 (J.C.). M.H.D. also acknowledges partial support from the College de France and from the French Agence Nationale de la Recherche.

Author Contributions

M.H.D. proposed the original idea for the device. A.K. developed the ideas and performed the theoretical analysis. J.C. contributed extensively to the discussions of the results. All authors contributed in writing the manuscript.

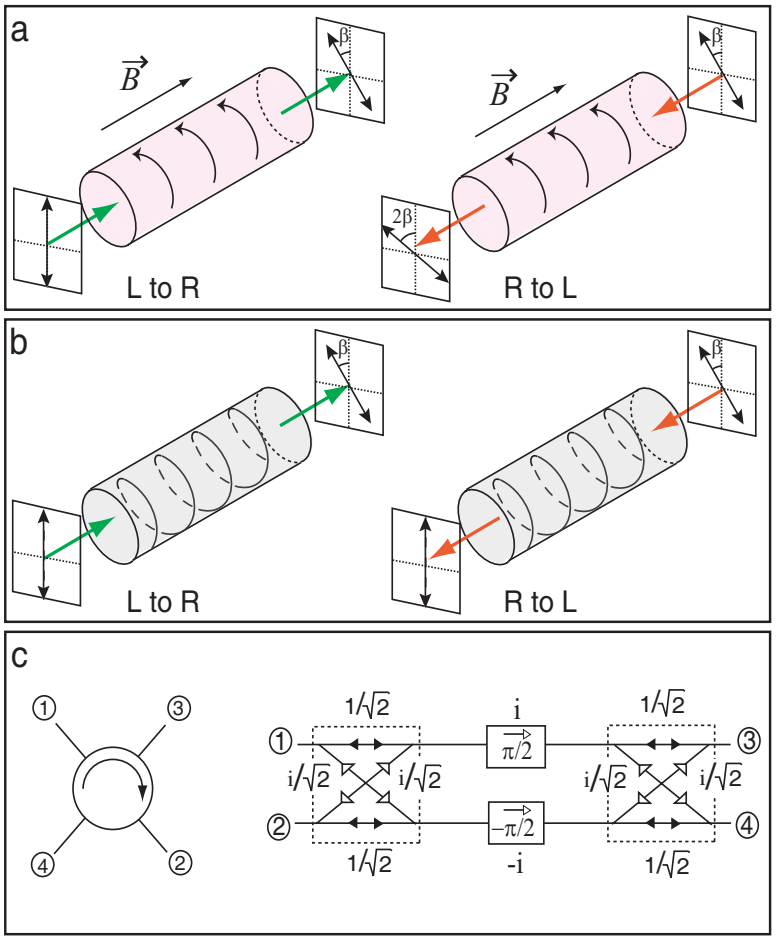

Figure 1: **Faraday rotation and circulator action. a,** Faraday rotation for a wave travelling from left to right in a Faraday-active medium, followed by a reflection back into the medium leading to a reversal of the direction of propagation. The rotation of the light polarization is fixed to a rotation-like property of the medium (shown by the arrows), set by an external magnetic field oriented along the propagation axis. The sense of light rotation as seen with respect to the direction of propagation remains the same, leading to the doubling of the rotation angle on reversing the ray through the medium. **b,** Rotation of the polarization vector of light on passage through an optically active medium, on the other hand, cancels out on reversing the direction of propagation. This occurs because optical rotation depends on the chirality of the medium (represented as a helix) which also reverses with the direction of propagation. **c,** Representation and schematic design of a conventional four-port circulator. The device consists of two 90 degree hybrids (equivalent to optical beam splitters) separated by a *non-reciprocal* phase shifter based on Faraday rotation. Solid black arrows indicate an amplitude split with no phase change while, open arrows indicate an amplitude split with a 90 degree phase change. The non-reciprocal phase shift is effective only for the propagation direction indicated by the arrow on the phase shifter box.

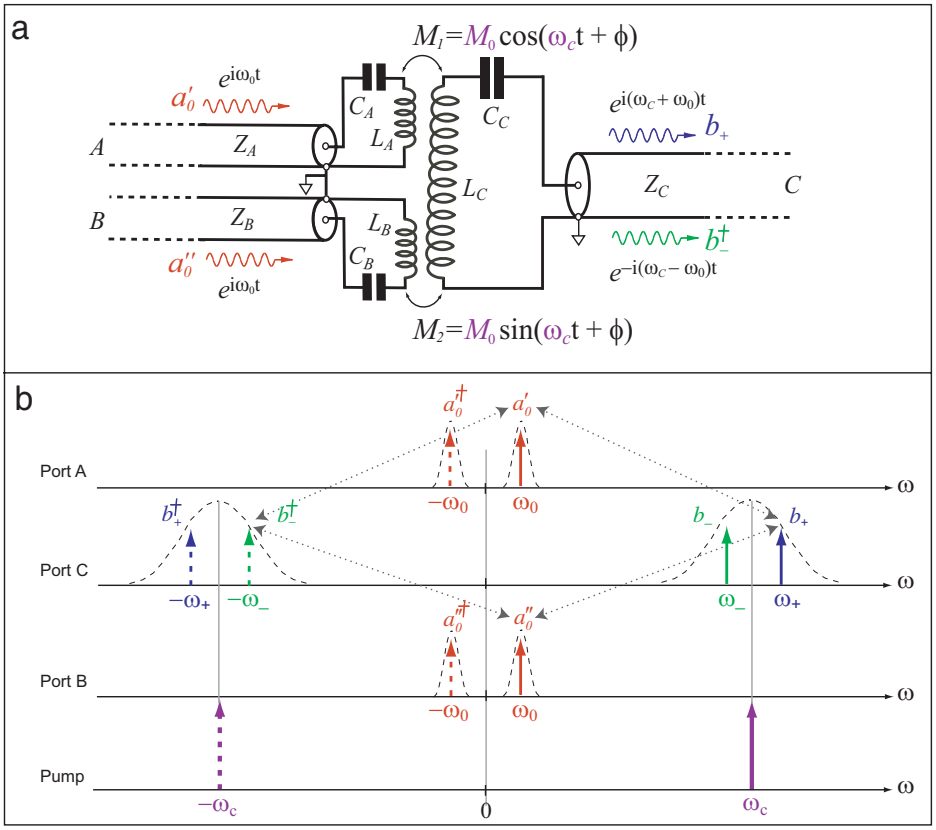

Figure 2: **Description of an active reversible (information-conserving) IQ modulator performing frequency up- and down-conversion (UDC). a,** Circuit schematic of the UDC containing only dispersive components. The two low frequency series LC resonators (with $L_A = L_B$ and $C_A = C_B$), are fed by two input semi-infinite transmission lines, A and B, and parametrically coupled to a third high frequency series LC resonator leading to an output line C. The parametric coupling is achieved by varying the mutual inductances M_1 and M_2 between the left and right resonators at the carrier frequency ω_c which, for optimal frequency conversion, is set at the band center of the right resonator. When operated from left to right, the circuit performs the modulation of low frequency signals of frequency ω_0 travelling on ports A and B to generate sidebands at $\omega_c \pm \omega_0$ travelling on the high frequency line C. It performs the inverse operation of demodulation when operated in reverse from right to left. **b,** Spectral density/response landscape for different spatial channels (or ports) of the UDC circuit in **a** as a function of frequency. The dotted lines represent the couplings between different ports. The solid and the dashed arrows represent different frequencies and respective conjugates. The resonance lineshapes of the two spatially distinct ports A and B are centered at $\omega_A = \omega_B = 1/\sqrt{L_{A,B}C_{A,B}}$. Here we show the case when the incoming signal at ω_0 is resonant with the center frequency ($\omega_0 = \omega_{A,B}$). The two sidebands generated by the UDC on channel C are detuned from the carrier ω_c by equal amounts.

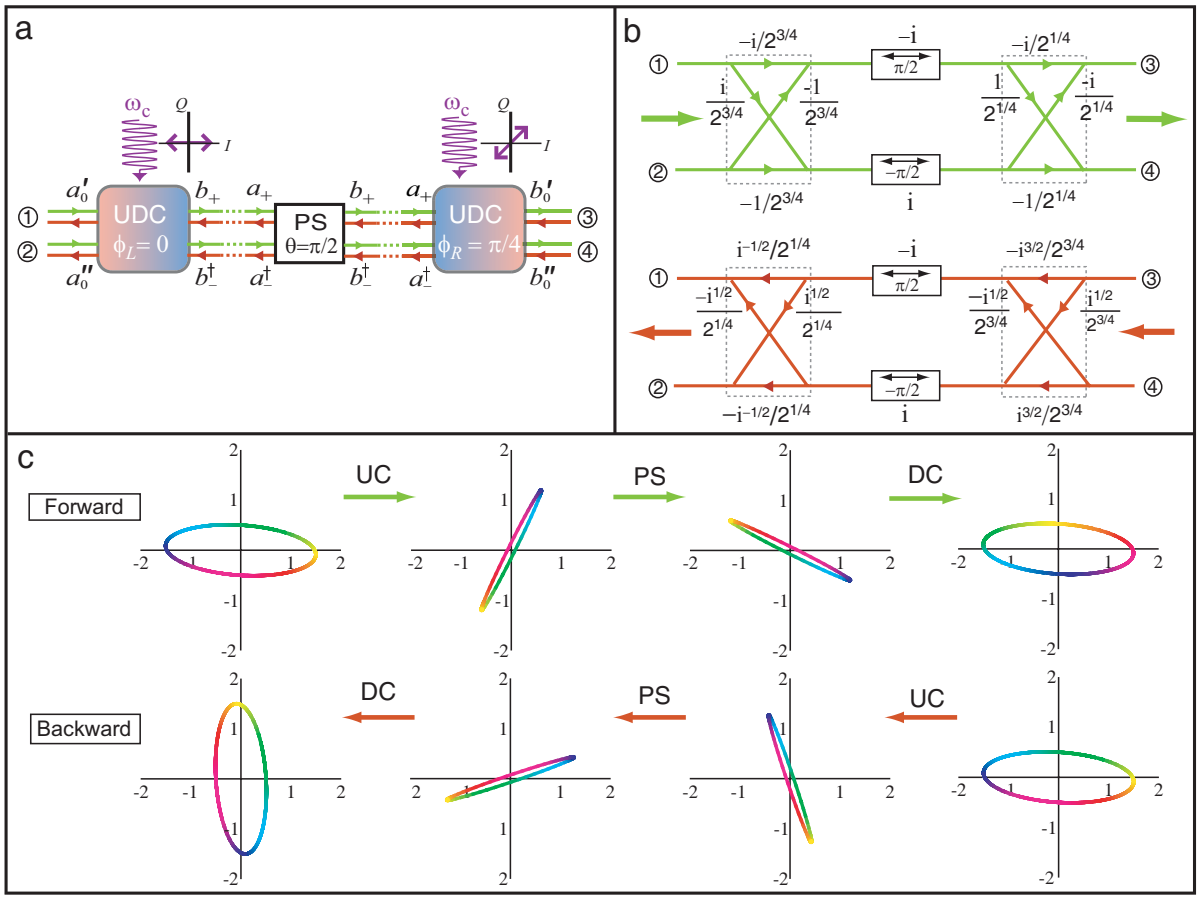

Figure 3: **Description of the active circulator. a,** Circuit schematic of the active circulator design: the first UDC stage acts as a frequency up-converter (UC) (also indicated by a gradation in the color of the relevant box) with a parametric coupling modulated at the carrier frequency $\omega_c = \omega_+ - \omega_0 = \omega_- + \omega_0$ and a phase $\phi_L = 0$. This is followed by a phase shifter (PS) that phase shifts both the sidebands by $\pi/2$, in opposite directions. They are then demodulated by the final UDC stage acting as a frequency down-converter (DC), with the carrier phase $\phi_R = \pi/4$. **b,** Forward (green) and backward (red) propagation diagrams calculated using transfer matrix method for **a** with appropriate choice of detuning ($\delta_\pm = 1/\sqrt{2}$) and coupling strengths ($\alpha_L = \alpha_R = 2^{-3/4}$) for maximum isolation. **c,** Representation of the device operation using modulation ellipses at each stage in the cascade. The top panel shows the forward propagation for the case when two distinct signals enter ports 1 and 2 respectively ($a_0^{'} = 1, a_0^{''} = 0.5e^{i\eta}$; $\eta = \pi/24$) while the bottom panel shows the backward propagation dynamics when the same signals enter ports 3 and 4 respectively ($b_0^{'} = 1, b_0^{''} = 0.5e^{i\eta}$). The relative phase and amplitudes are chosen to represent the most general case of two input signals which differ in both amplitude and phase. The relative phase difference between the two signals is encoded as the tilt of the modulation ellipse in the IQ plane while their average phase is represented as the color along the perimeter of the ellipse with yellow indicating zero phase (also see supplementary information for more details).

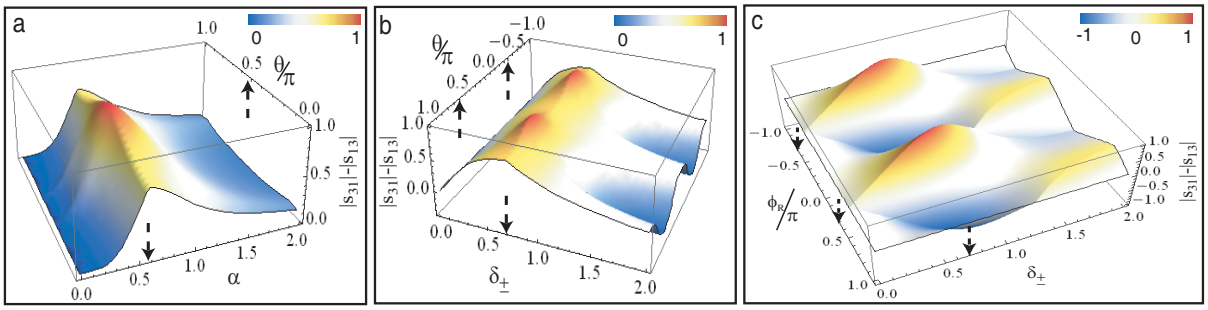

Figure 4: **Variation of the difference between forward and backward transmission coefficients ($|s_{31}| - |s_{13}|$).** Asymmetry in transmission, calculated for coupling angles $\phi_L = 0$ and $\phi_R = \pi/4$, as a function of **a,** strength of the coupling α and phase rotation θ performed by the second phase shifting stage, **b,** detuning $\delta_\pm$ of the sidebands from the carrier and phase rotation θ, and **c,** detuning $\delta_\pm$ and the phase of the pump at second UDC stage ϕ_R. The points of maxima correspond to the ideal values reported in the text. The plot in **b**, also shows the periodicity of the response of the device as a function of θ. In **c**, the variation with respect to the pump phase shows the reversal of transmission characteristics with $\phi_R \to -\phi_R$. As in **b**, the response is periodic in ϕ_R with a period equal to π. It can be seen that the design continues to work for moderate deviations from the preferred phase angle $\theta = \pi/2$, coupling $\alpha_{L,R} = 2^{-3/4}$, detuning $\delta_\pm = 1/\sqrt{2}$ and pump phase $\phi_R = \pi/4$ (values indicated with dashed arrows along the axis).

Supplementary Information for Noiseless Nonreciprocity in a Parametric Active Device

Archana Kamal,[1] John Clarke,[2] Michel Devoret[1*]

[1]Department of Physics and Applied Physics, Yale University,
15 Prospect Street, New Haven, CT 06520, USA
[2]Department of Physics, University of California, and Materials Sciences Division,
Lawrence Berkeley National Laboratory, Berkeley, CA 94720, USA

Methods

Derivation of scattering matrix. In this section, we present the details of the derivation of the scattering matrix S for the UDC stage. A scattering matrix has the general form

$$\vec{a}[\omega]^{\rm out} = S[\omega, \omega']\vec{a}^{\rm in}[\omega'], \tag{S1}$$

where $\vec{a}^{\rm in/out}$ is a column vector formed by the reduced mode amplitudes (in terms of photon number at the relevant frequencies) of the network. This description extends to all the spatial *and* temporal modes of the network. A convenient and simple way of deriving the S matrix involves calculating the impedance matrix Z using usual circuit theory, and then using the identity [1]

$$S = (Z + Z_0)^{-1}.(Z - Z_0) \tag{S2}$$

to obtain the S matrix. Here Z_0 denotes the characteristic impedance of the transmission lines acting as channels for propagation of the incoming and outgoing signals at various ports. It is

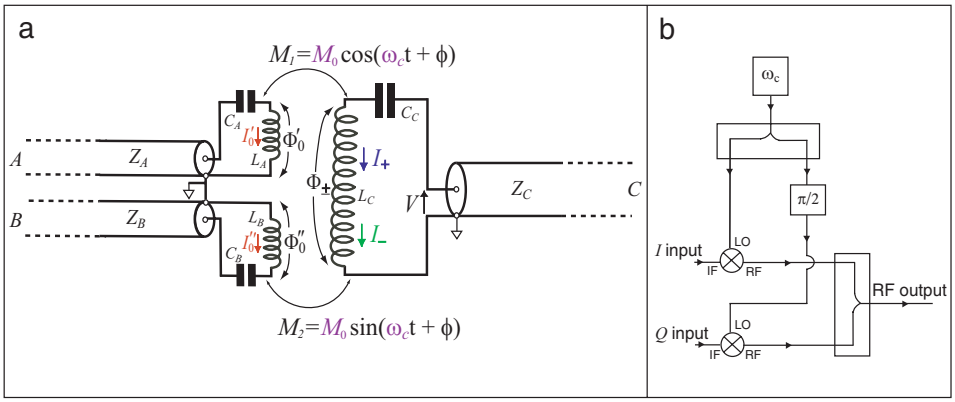

Figure S1: **Comparison of two IQ modulation schemes: a** Detailed circuit schematic of the UDC performing reversible IQ modulation. The fluxes across different inductances denoted as Φ_i and the respective mode currents denoted as I_i are shown for each series LC resonator. The mutual inductances $M_1,\ M_2$ lead to off-diagonal coupling (mixing) between the current of the left resonators and the flux across the inductance of the right resonator and vice versa. **b,** Block diagram of a non-reversible circuit performing the operation described in **a**. The circuit employs dissipative components like the mixers (represented by the cross in circle symbol). The CW tone from the generator imposing a carrier frequency ω_c is split into two copies, one phase shifted by $\pi/2$ with respect to the other. The carrier is modulated by the signal at ω_0 and encoded on two separate channels: the 'in phase" (or I) component and the "quadrature" (or Q) component. The I and Q channels are then combined to propagate onto a single spatial channel.

of the form

$$Z_0 = \mathrm{diag}(Z_A, Z_B, Z_C, Z_C), \tag{S3}$$

where $Z_A = Z_B$ and Z_C are characteristic impedances of the semi-infinite transmission lines addressing the low and high frequency ports respectively.

For the parametrically coupled series LC oscillators forming the UDC stage, Fig. S1a, we obtain the total impedance matrix Z by adding the inductive (Z_{ind}) and capacitive (Z_{cap}) contributions respectively. The inductance matrix L defines the constitutive relationship between the currents and fluxes for different inductances of the circuit:

$$\begin{pmatrix} \Phi_0'(t) \\ \Phi_0''(t) \\ \Phi_+(t) \\ \Phi_-(t) \end{pmatrix} = \begin{pmatrix} L_A & 0 & M_0 e^{-i\phi} & M_0 e^{i\phi} \\ 0 & L_B & iM_0 e^{-i\phi} & -iM_0 e^{i\phi} \\ M_0 e^{i\phi} & -iM_0 e^{i\phi} & L_C & 0 \\ M_0 e^{-i\phi} & iM_0 e^{-i\phi} & 0 & L_C \end{pmatrix} \begin{pmatrix} I_0'(t) \\ I_0''(t) \\ I_+(t) \\ I_-(t) \end{pmatrix} \tag{S4}$$

$$= \quad L \begin{pmatrix} I_0^{'}(t) \\ I_0^{''}(t) \\ I_+(t) \\ I_-(t) \end{pmatrix}. \tag{S5}$$

In writing the above matrix, we ignore the fluxes at higher harmonics of the modes at ω_0 and $\omega_\pm$. The inductive contribution to the impedance is then calculated by using the identity

$$\begin{pmatrix} V_0^{'} \\ V_0^{''} \\ V_+ \\ V_- \end{pmatrix} = \begin{pmatrix} \dot{\Phi}_0^{'} \\ \dot{\Phi}_0^{''} \\ \dot{\Phi}_+ \\ \dot{\Phi}_- \end{pmatrix} = L\frac{d}{dt} \begin{pmatrix} I_0^{'} \\ I_0^{''} \\ I_+ \\ I_- \end{pmatrix} \tag{S6}$$

$$\Rightarrow \qquad V[\omega] = Z_{\rm ind} I[\omega]$$

where the subscripts denote the relevant frequency modes. It is straightforward to define the capacitance matrix for the circuit in the same manner:

$$\begin{pmatrix} V_0^{'} \\ V_0^{''} \\ V_+ \\ V_- \end{pmatrix} = (-j\omega)^{-1} \begin{pmatrix} C_A^{-1} & 0 & 0 & 0 \\ 0 & C_B^{-1} & 0 & 0 \\ 0 & 0 & C_C^{-1} & 0 \\ 0 & 0 & 0 & -C_C^{-1} \end{pmatrix} \begin{pmatrix} I_0^{'} \\ I_0^{''} \\ I_+ \\ I_- \end{pmatrix} \tag{S7}$$

$$\Rightarrow \qquad V[\omega] = Z_{\rm cap} I[\omega]$$

The extra negative sign in s_{44} of Eq. (S7) accounts for the generation of the conjugate wave amplitude $a^\dagger[\omega_-]$ as a result of mixing of carrier ω_c and signal ω_0. Hence, on taking the Fourier transform of the current and voltage vectors, an extra negative sign appears for the corresponding coefficient in $Z_{\rm cap}$. The total Z matrix can then be written as

$$Z = Z_{\rm ind} + Z_{\rm cap}, \tag{S8}$$

which gives

$$Z = \begin{pmatrix} -i\delta_0 Z_{A,B} & 0 & -i\alpha Z_C e^{-i\phi} & -i\alpha Z_C e^{i\phi} \\ 0 & -i\delta_0 Z_{A,B} & \alpha Z_C e^{-i\phi} & -\alpha Z_C e^{i\phi} \\ -i\alpha Z_{A,B} e^{i\phi} & -\alpha Z_{A,B} e^{i\phi} & -i\delta_\pm Z_C & 0 \\ i\alpha Z_{A,B} e^{-i\phi} & -\alpha Z_{A,B} e^{-i\phi} & 0 & -i\delta_\pm Z_C \end{pmatrix}. \tag{S9}$$

Here we have introduced the symbols

$$\delta_0 = \frac{|\omega_0 - \omega_{A,B}|}{\Gamma_{A,B}}; \quad \Gamma_{A,B} = \frac{Z_{A,B}}{2L_{A,B}}$$

$$\delta_\pm = \frac{|\omega_\pm - \omega_C|}{\Gamma_C}; \quad \Gamma_C = \frac{Z_C}{2L_C}$$
$$\alpha = \frac{M_0}{\sqrt{L_{A,B}L_C}},$$

with Γ_i denoting the linewidth of the i^{th} resonator. On using Eqs. (S9) and (S3) in Eq. (S2), we obtain

$$\begin{pmatrix} a_0^{'\text{out}} \\ a_0^{''\text{out}} \\ b_+^{\text{out}} \\ b_-^{\dagger\text{out}} \end{pmatrix} = \begin{pmatrix} r_0 & -q_0 & t_d e^{-i\phi} & s_d e^{i\phi} \\ q_0 & r_0 & it_d e^{-i\phi} & -is_d e^{i\phi} \\ t_u e^{i\phi} & -it_u e^{i\phi} & r_+ & 0 \\ -s_u e^{-i\phi} & -is_u e^{-i\phi} & 0 & r_- \end{pmatrix} \begin{pmatrix} a_0^{'\text{in}} \\ a_0^{''\text{in}} \\ b_+^{\text{in}} \\ b_-^{\dagger\text{in}} \end{pmatrix} \tag{S10}$$

$$= S \begin{pmatrix} a_0^{'\text{in}} \\ a_0^{''\text{in}} \\ b_+^{\text{in}} \\ b_-^{\dagger\text{in}} \end{pmatrix}, \tag{S11}$$

where $a_i^{\text{in/out}}$ denotes the shorthand notation for $a[\omega_i]^{\text{in/out}}$ [cf. Eq. (S1)]. The symbols a, b denote the wave amplitudes for left and right ports respectively. The detailed expressions for scattering coefficients are listed below:

$$r_0 = \frac{(\delta_0^2+1)(\delta_\pm+i)^2 - 4\alpha^4}{(\delta_0+i)^2(\delta_\pm+i)^2 - 4\alpha^4}; \quad q_0 = \frac{4\alpha^2(\delta_\pm+i)}{(\delta_0+i)^2(\delta_\pm+i)^2 - 4\alpha^4}; \tag{S12}$$

$$r_+ = \frac{(\delta_0+i)(\delta_\pm-i) - 2\alpha^2}{(\delta_0+i)(\delta_\pm+i) - 2\alpha^2}; \quad r_- = \frac{(\delta_0+i)(\delta_\pm-i) + 2\alpha^2}{(\delta_0+i)(\delta_\pm+i) + 2\alpha^2}; \tag{S13}$$

$$t_u = i\left(\frac{Z_C}{Z_{A,B}}\right)\left(\frac{2\alpha}{(\delta_0+i)(\delta_\pm+i) - 2\alpha^2}\right); \tag{S14}$$

$$s_u = i\left(\frac{Z_C}{Z_{A,B}}\right)\left(\frac{2\alpha}{(\delta_0+i)(\delta_\pm+i) + 2\alpha^2}\right); \tag{S15}$$

$$t_d = i\left(\frac{Z_{A,B}}{Z_C}\right)\left(\frac{2\alpha}{(\delta_0+i)(\delta_\pm+i) - 2\alpha^2}\right); \tag{S16}$$

$$s_d = i\left(\frac{Z_{A,B}}{Z_C}\right)\left(\frac{2\alpha}{(\delta_0+i)(\delta_\pm+i) + 2\alpha^2}\right). \tag{S17}$$

Equations (S12)-(S17) show that the effective coupling strength α plays the role of the parametric drive ("pump") in the UDC. In the limit $\alpha = 0$, transmission coefficients t_i and s_i become identically zero while the reflection coefficients r_i reduce to those for three independent series LCR circuits with resonance frequencies ω_0 and ω_c respectively.

We note that the matrix in Eq. (S11) is one of the block diagonals of the full 8×8 scattering matrix that describes the interaction of both the positive and negative frequency wave amplitudes for all participating modes:

$$\begin{pmatrix} a_1^{\text{out}} \\ a_1^{\dagger\text{out}} \\ a_2^{\text{out}} \\ a_2^{\dagger\text{out}} \\ \vdots \end{pmatrix} = \tilde{S} \begin{pmatrix} s_{11} & 0 & \dots & \dots \\ 0 & s_{11}^* & \dots & \dots \\ \vdots & \vdots & \ddots & \vdots \\ s_{2N,1} & \dots & \dots & s_{2N,2N} \end{pmatrix} \begin{pmatrix} a_1^{\text{in}} \\ a_1^{\dagger\text{in}} \\ \vdots \\ a_{2N}^{\dagger\text{in}} \end{pmatrix}. \tag{S18}$$

This is especially important in the case of an active network where a conjugation operation is possible i.e. $a_i \mapsto a_i^\dagger = a[-\omega_i]$. The full scattering matrix $\tilde{S}$ satisfies the following general properties:

1. det($\tilde{S}$) =1 (as det (S) =1)
2. $\sum_{j=1}^{4} |s_{ij}|^2 = 1$
3. $\tilde{S}^T J \tilde{S} = J$,

where J represents a symplectic structure defined on the $2N \times 2N$ phase space (N = number of degrees of freedom),

$$J = i\sigma_Y \otimes I_N. \tag{S19}$$

The last condition of symplecticity follows from the fact that a transformation of the modes as performed by the scattering matrix needs to be a canonical transformation. This requirement translates into the condition for preservation of phase space volume (information) or the number of participating modes (degrees of freedom) in the system.

Derivation of transfer matrix. In this section, we derive the transfer matrix for the UDC stage. This description is equivalent to the usual $ABCD$ matrix of the circuit theory defined in terms of the voltages and currents for a two-port network [1],

$$\begin{pmatrix} V_b \\ I_b \end{pmatrix} = \begin{pmatrix} A & B \\ C & D \end{pmatrix} \begin{pmatrix} V_a \\ I_a \end{pmatrix}. \tag{S20}$$

As there exists a straightforward mapping between the reduced wave amplitudes a_i introduced earlier, and the currents and voltages at the ports [2],

$$a_i^{\text{out}} = \frac{V_i + Z_0 I_i}{\sqrt{2Z_0\hbar\omega_i}} \tag{S21}$$

$$a_i^{\text{in}} = \frac{V_i - Z_0 I_i}{\sqrt{2Z_0\hbar\omega_i}}, \tag{S22}$$

we can easily adapt the concept to the above choice of variables.

For the cascaded chain, we first evaluate the transfer matrix of each stage and then multiply them to obtain the total transfer matrix of the cascade. For the UDC stage performing up-conversion, we can find the relevant transfer matrix by solving Eq. (S11) to obtain sideband amplitudes $(a_+, a_-^\dagger)$ in terms of low frequency amplitudes $(a_0^{'}, a_0^{''})$

$$\begin{pmatrix} b_+^{\text{out}} \\ b_+^{\text{in}} \\ b_-^{\dagger\text{out}} \\ b_-^{\dagger\text{in}} \end{pmatrix} = T \begin{pmatrix} a_0^{'\text{in}} \\ a_0^{'\text{out}} \\ a_0^{''\text{in}} \\ a_0^{''\text{out}} \end{pmatrix}. \tag{S23}$$

The reversal of 'in' and 'out' in the column vectors on left and right hand sides of Eq. (S23) is required to maintain a consistent sense of propagation through the device as the output of the $(N-1)^{th}$ stage acts as the input for the N^{th} stage in the chain. On doing the above transformation, we obtain

$$T_{UC} = \begin{pmatrix} t_{+,LR}e^{i\phi} & t_{+,RL}^* e^{i\phi} & -it_{+,LR}e^{i\phi} & it_{+,RL}^* e^{i\phi} \\ t_{+,RL}e^{i\phi} & t_{+,LR}^* e^{i\phi} & -it_{+,RL}e^{i\phi} & it_{+,LR}^* e^{i\phi} \\ t_{-,LR}e^{-i\phi} & t_{-,RL}^* e^{-i\phi} & it_{-,LR}e^{-i\phi} & it_{-,RL}^* e^{-i\phi} \\ t_{-,RL}e^{-i\phi} & t_{-,LR}^* e^{-i\phi} & it_{-,RL}e^{-i\phi} & it_{-,LR}^* e^{-i\phi} \end{pmatrix}, \tag{S24}$$

with

$$t_{+,LR} = i\left(\frac{Z_{A,B}}{Z_C}\right)\left(\frac{(\delta_0 - i)(\delta_\pm - i) - 2\alpha^2}{4\alpha}\right)$$

$$t_{+,RL} = i\left(\frac{Z_{A,B}}{Z_C}\right)\left(\frac{(\delta_0 - i)(\delta_\pm + i) - 2\alpha^2}{4\alpha}\right)$$

$$t_{-,LR} = i\left(\frac{Z_{A,B}}{Z_C}\right)\left(\frac{(\delta_0 - i)(\delta_\pm - i) + 2\alpha^2}{4\alpha}\right)$$

$$t_{-,RL} = i\left(\frac{Z_{A,B}}{Z_C}\right)\left(\frac{(\delta_0 - i)(\delta_\pm + i) + 2\alpha^2}{4\alpha}\right).$$

The subscripts (+,-) refer to the resultant sideband generated at the output (ω_+ or ω_-^*) while $LR(RL)$ indicates the relevant direction of propagation as *left-to-right* (*right-to-left*). We note that the condition for the transformation describing the mapping between S and T matrices to be non-singular is

$$s_{13}s_{24} - s_{23}s_{14} \neq 0. \tag{S25}$$

This condition is violated when the couplings M_1, M_2 (Fig. S1) are in phase and hence a transfer matrix cannot be defined in such a case.

Similarly, the scattering matrix of the phase shifting stage,

$$PS = \begin{pmatrix} 0 & 0 & e^{-i\theta} & 0 \\ 0 & 0 & 0 & e^{i\theta} \\ e^{-i\theta} & 0 & 0 & 0 \\ 0 & e^{i\theta} & 0 & 0 \end{pmatrix}, \tag{S26}$$

yields a transfer matrix of the form

$$T_{PS} = \begin{pmatrix} e^{-i\theta} & 0 & 0 & 0 \\ 0 & e^{i\theta} & 0 & 0 \\ 0 & 0 & e^{i\theta} & 0 \\ 0 & 0 & 0 & e^{-i\theta} \end{pmatrix}. \tag{S27}$$

Finally, by exploiting the fact that down-conversion is just the inverse operation of the phenomenon of up-conversion we obtain the transfer matrix of the second UDC stage as

$$T_{DC} = F \times T_{UC}^{-1} \times F, \tag{S28}$$

where F is the flip matrix of the form $F = i\sigma_X \otimes I_2$ required to preserve the consistency in labelling the input and output amplitudes. The forward and backward propagation diagrams in Fig. 3b of the main text have been calculated using the matrices T_{UC} [Eq. (S24)] and T_{DC} [Eq. (S28)]. Each arm of the propagation diagram notes the net forward going amplitude at that frequency: for instance, the amplitudes for first UDC stage performing upconversion in the forward propagation diagram (green) can be evaluated using the first and third rows of the matrix in Eq. (S24) with $\phi = 0$. The net forward going amplitude contributed by $a_0^{'}$ to a_+

can be calculated as $t_{11} - t_{12} = (t_{+,LR} - t^*_{+,RL}) = -i/2^{3/4}$ while that due to $a_0^{''}$ is given by $t_{13} - t_{14} = (-it_{+,LR} - it^*_{+,RL}) = -1/2^{3/4}$, evaluated for the optimal parameter values $\delta_0 = 0$, $\delta_\pm = 1/\sqrt{2}$, $\alpha = 1/2^{3/4}$ reported in the main text. For the backward propagation, a similar exercise using the second and fourth rows of T_{UC} (and T_{DC}) leads to the propagation diagram shown in the lower panel of Fig. 3b in red.

The total transfer matrix

$$T_{\text{total}} = T_{DC_2}(\phi = \pi/4) \times T_{PS}(\theta = \pi/2) \times T_{UC_1}(\phi = 0) \tag{S29}$$

establishes the relationship between the low frequency signals on the left and the right ports of the cascade as

$$\begin{pmatrix} b_0^{'\text{out}} \\ b_0^{'\text{in}} \\ b_0^{''\text{out}} \\ b_0^{''\text{in}} \end{pmatrix} = \begin{pmatrix} i & 0 & 0 & 0 \\ 0 & 0 & 0 & i \\ 0 & 0 & i & 0 \\ 0 & -i & 0 & 0 \end{pmatrix} \begin{pmatrix} a_0^{'\text{in}} \\ a_0^{'\text{out}} \\ a_0^{''\text{in}} \\ a_0^{''\text{out}} \end{pmatrix} \tag{S30}$$

$$= T_{\text{total}} \begin{pmatrix} a_0^{'\text{in}} \\ a_0^{'\text{out}} \\ a_0^{''\text{in}} \\ a_0^{''\text{out}} \end{pmatrix}. \tag{S31}$$

The matrix in Eq. (S30) has been evaluated for the resonant case $\delta_0 = 0$ and the parameter values

$$\delta_\pm = \frac{1}{\sqrt{2}}; \quad \alpha = \frac{1}{2^{3/4}}. \tag{S32}$$

On evaluating the total scattering matrix S_{total} from T_{total}, we obtain the four port circulator reported in Eq. (9) of the main text. The device behaves nonreciprocally since $S^T \neq S$ [1].

Modulation ellipse. This scheme, providing a geometrical visualization of the action of our device, represents the superposition of two sinusoidal signals as an ellipse in the plane defined by the quadratures I and Q. In general for any two complex phasors $\vec{a}$ and $\vec{b}$ rotating in opposite

directions

$$\vec{a}e^{i\omega t} + \vec{b}e^{-i\omega t} \;=\; \underbrace{\mathrm{Re}[(\vec{a}+\vec{b}^{*})e^{i\omega t}]}_{I} \;+\; i\,\underbrace{\mathrm{Im}[(\vec{a}-\vec{b}^{*})e^{i\omega t}]}_{Q}. \tag{S33}$$

The magnitudes and phases of the two complex signals (4 quantities in total) are encoded as different properties of a colored ellipse in the IQ plane: the semi-major axis of the ellipse equals $\rho_+ = |a| + |b|$ while the semi minor axis equals $\rho_- = ||a| - |b||$, the angle with the I axis equals $(\theta_a - \theta_b)/2$ and the location of the colors on the ellipse represents the phase angle $(\theta_a + \theta_b)/2$.

The output at each stage in the active circulator comprises two modes – the spatially orthogonal modes $(a_0^{'}, a_0^{''})$ and the sidebands (a_+, a_-) that can be represented as phasors with opposite sense of rotations in a frame rotating at the carrier frequency ω_c. Thus we can faithfully map the detailed dynamics of the device after each stage using the modulation ellipse representation and plot the combined output signal in the IQ plane with $I = \mathrm{Re}[(a+b)e^{i\omega t}]$ and $Q = \mathrm{Im}[(a-b)e^{i\omega t}]$ (a and b representing the relevant modes at each stage).

Now we present examples of two different kinds of phase rotations and the resultant transformations ("rotations") of the modulation ellipse (see Fig. S3 for additional examples on modulation ellipse representation).

1. Phase shift:

   The action of a phase shifter which performs frequency independent phase rotations of both the phasors can be described using the transformations:

   $$a \mapsto ae^{i\theta} \quad \text{and} \quad b \mapsto be^{i\theta}. \tag{S34}$$

   On using the above and performing the analysis in the IQ plane, we obtain the expressions for new coordinates as

   $$I = \mathrm{Re}[ae^{i(\omega t+\theta)} + b^{*}e^{i(\omega t-\theta)}] \tag{S35}$$

$$Q = \mathrm{Im}[ae^{i(\omega t+\theta)} - b^* e^{i(\omega t-\theta)}]. \tag{S36}$$

The action of such an operation can be easily visualized using the modulation ellipse as shown in Fig. S2(e).

2. Free evolution:

   In contrast to the transformation described above, we now consider the rotation preformed by a mere time evolution of the two counter-rotating phasors (say by passage through a transmission line). In such a case, the phases of the two signals continue to evolve in opposite directions collecting a phase δ in time t ($\delta = \omega t$),

$$a \mapsto ae^{+i\delta} \quad \text{and} \quad b \mapsto be^{-i\delta}. \tag{S37}$$

   The IQ coordinates are calculated as

$$I = \mathrm{Re}[(a + b^*)e^{i(\omega t+\delta)}] \tag{S38}$$

$$Q = \mathrm{Im}[(a - b^*)e^{i(\omega t+\delta)}]. \tag{S39}$$

   It is immediately evident, that under time evolution, there is only a trivial phase accumulation leading to change of relative positions of the two phasors along the circumference of the modulation ellipse with no rigid rotation of the ellipse, Fig. S2(f).

In Fig. 3C of the main text, we have used modulation ellipses to represent the dynamics at each stage of the active circulator. In the forward propagation direction (L to R), the output ellipse representing ports 3 and 4 has the same orientation as the input ellipse representing ports 1 and 2; only the average phase of the total output changes as indicated by the change of color along the circumference of the output ellipse. In the backward propagation direction (R to L), however, the ellipse obtained at ports 1 and 2 is rotated by $\pi/2$ with respect to the input ellipse of ports 3 and 4, in addition to the trivial average phase change. This indicates the swapping of

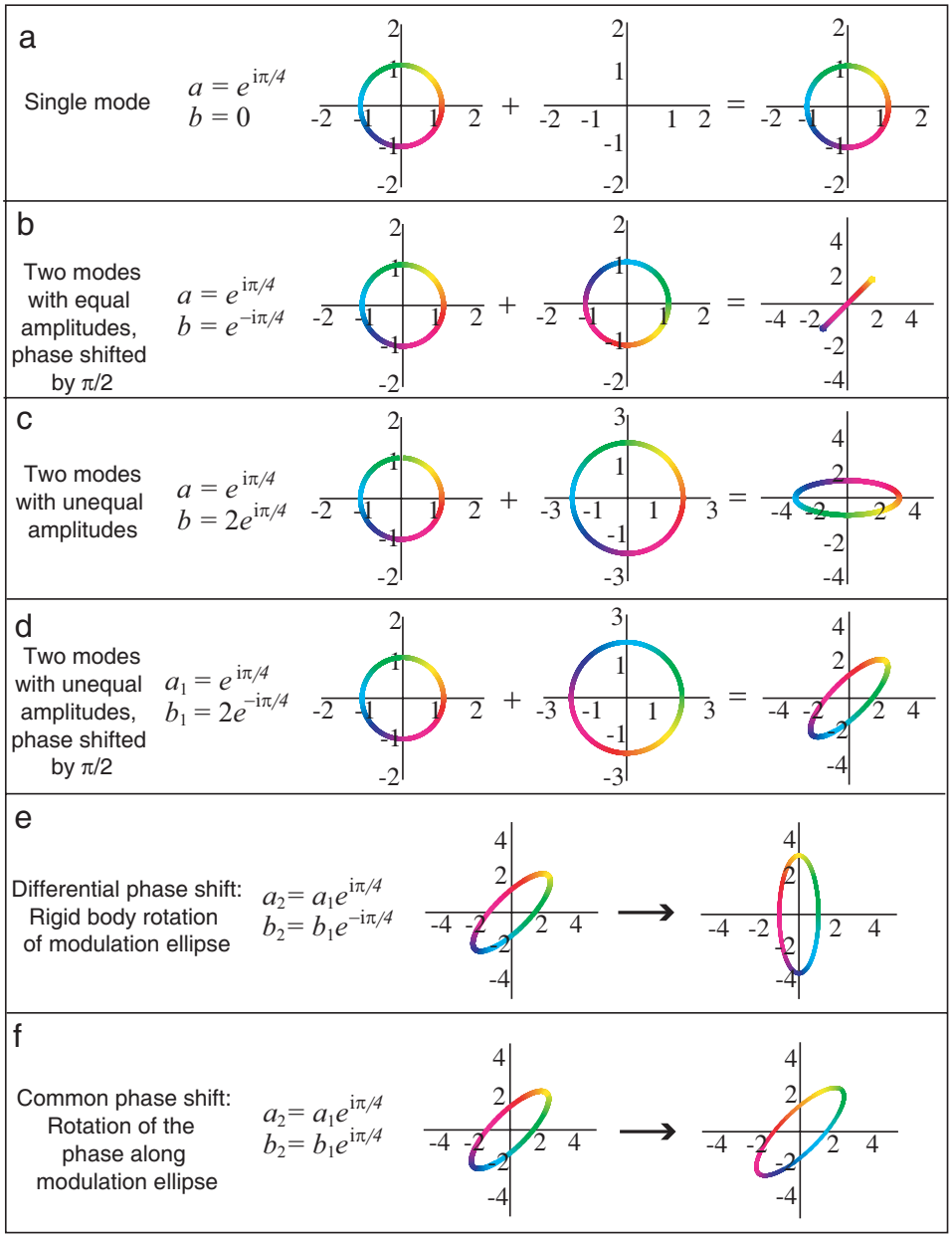

Figure S2: **Modulation ellipse representation of two phasors.** In each of the panels, the first column describes the phasors under consideration, the second column gives a precise mathematical formula for them and the third column shows the corresponding modulation ellipse. In **a-d**, we show both the input modes and the resultant modulation ellipse. The tilt of the ellipse with respect to the I axis represents the relative phase between the two modes $[(\theta_a - \theta_b)/2]$ while the color along the ellipse represents the average initial phase of the two modes $[(\theta_a + \theta_b)/2]$, with yellow representing the position of 0 (or 2π). Figs. **(e)** and **(f)** represent the resulting ellipses on performing the indicated transformations on the ellipse in **(d)**.

the transmitted amplitudes – port 1 (port 2) receiving the input at port 4 (port 3) – that leads to nonreciprocal transmission characteristics of the device.

References

[1] Pozar, David M. *Microwave Engineering* (Wiley, ed. 3, 2005), pp.471-482.

[2] Kamal, A., Marblestone, A. & Devoret, M. H. *Phys. Rev. B* **79**, 184301 (2009).